Supplementary Appendix

This appendix has been provided by the authors to give readers additional information about their work.

Supplement to: Vilboux T, Lev A, Malicdan MCV, et al. A congenital neutrophil defect syndrome associated with mutations in *VPS45*. N Engl J Med 2013;369:54-65. DOI: 10.1056/NEJMoa1301296

SUPPLEMENTARY APPENDIX

A Congenital Neutrophil Defect Syndrome Associated With Mutations In *VPS45*

Thierry Vilboux, Atar Lev, May Christine V Malicdan, Amos J. Simon, et al.

AUTHORS' CONTRIBUTIONS

Thierry Vilboux, Atar Lev, Amos J. Simon, Yair Anikster, Christoph Klein, William A. Gahl and Raz Somech designed the study.

Päivi Järvinen, Tomas Racek, Jacek Puchałka, Ben Zion Garty, Osama M. Atawneh, Jutte van der Werff ten Bosch, Amos Toren, Andrew Cullinane,Christoph Klein and Raz Somech gathered the data.

Thierry Vilboux, Atar Lev, May Christine V Malicdan, Amos J. Simon, Päivi Järvinen, Tomas Racek, Jacek Puchałka, Raman Sood, Blake Carrington, Kevin Bishop, James Mullikin, Marjan Huizing, Eran Eyal, Baruch Wolach, Ronit Gavrieli, Andrew Cullinane, Michalle Soudack, Tatiana Babushkin, Ginette Schiby, Camila Avivi, Sylvie Polak-Charcon, Iris Barshack, Ninette Amariglio, Gideon Rechavi, Jutte van der Werff ten Bosch, Christoph Klein, William A. Gahl and Raz Somech analyzed the data.

All the Authors vouch for the data and the analysis.

Atar Lev, Amos J. Simon and Raz Somech wrote the first draft of the paper.

Atar Lev, Amos J. Simon, Gideon Rechavi, Christoph Klein, William A. Gahl and Raz Somech wrote the paper.

All the Authors agreed to publish the paper.

SUPPLEMENTARY METHODS

Sequencing

The GAIIx sequencer (Illumina) [1] employed 101-bp paired-end read sequencing. Image analysis and base calling were performed using Illumina Genome Analyzer Pipeline software (versions 1.4.0 or greater) with default parameters. Reads were aligned to a human reference sequence (UCSC assembly hg18, NCBI build 36) using a package called Efficient Large-scale Alignment of Nucleotide Databases (Illumina, San Diego, CA). Genotypes were called at all positions where there were high-quality sequence bases using a Bayesian algorithm called the Most Probable Genotype [2] and variants were filtered using the graphical software tool VarSifter v1.3. [3] The database dbSNP (http://www.ncbi.nlm.nih.gov/snp/) covers the 1.22% of the human genome corresponding to the Consensus Conserved Domain Sequences and more than 1,000 non-coding RNAs. [4]

VPS45 mutation genotyping

For dideoxy sequencing of *VPS45*, PCR amplification products were directly sequenced using BigDye 3.1 Terminator chemistry (Applied Biosystems) and separated on an ABI 3130xl genetic analyzer (Applied Biosystems). Data were evaluated using Sequencer v5.0 software (Gene Codes Corporation, Ann Arbor, MI). 125 ethnically matched healthy controls were examined for the *VPS45* mutated and wild type alleles using the TaqMan Pre-Designed SNP Genotyping Assay (Applied Biosystems). The assay contained forward and reverse primers, flanking the mutated nucleotide and 2 labeled probes, VIC dye-MGB and 6FAM™ dye-MGB, each bound preferentially to one of the alleles. The

reaction was performed using the ABI-7900 Sequence Detection System (Applied Biosystems). Results were analyzed with the comparative C_T method as described.[5]

Modeling

The template structure for VPS45 modeling was UNC18 (pdb code 2xhe chain A) from *Monosiga brevicollis.* [6] We used Modeller,[7,8] which is based on distance constraints, to construct the model. SCCOMP [9] was used to obtain models for the Thr224Asn and Glu238Lys mutants based on the VPS45 model. No backbone changes were introduced, and we used the option to model all residues having direct contact with the mutations. Various tools predicted thermostability and function of the VPS45 mutants are listed in Table S2.Of those, 12 are based on structure input and were fed with the 3D model we created. These programs use elaborated structural features and chemical interactions and can incorporate contact potentials. We also used 5 methods that apply only for sequence/conservation information. Jmol [10] and chimera [11] were used for visualization and to create images.

Neutrophil studies

Superoxide production was measured as superoxide dismutase-inhibitable reduction of ferricytochrome *c*. Hydrogen peroxide production was measured with the DHR-1,2,3 assay (Sigma-Aldrich, St. Louis, Mo). In both assays neutrophils were stimulated by PMA (Phorbol Miristate Acetate, Sigma-Aldrich, St. Louis, MO). Immuno blotting was performed for protein analysis of the NADPH-oxidase subunits, using mouse monoclonal antibodies against $gp91^{phox}$ (mAb 48) and $p22^{phox}$ (mAb 449) (A generous gift from Prof.

Dirk Ross), and specific rabbit antisera against $p47^{phox}$ (A generous gift from Prof. Edgar Pick) and $p67^{phox}$ (Santa Cruz Biotechnology). Chemotaxis was assessed in a 48-well chemotaxis chamber through a 3-μm pore size filter [12,13] and induced by 1 μM of the chemoattractant N-formyl-Met-Leu-Phe (fMLP), IL8 or zymosan activated serum (Sigma-Aldrich, St. Louis, MO). Random migration was conducted in the presence of M199 medium (Biological Industries). Net chemotaxis was calculated by subtracting the random from the chemotactic migration (fMLP-stimulated neutrophils). All procedures were performed in quadruplicate.

Electron microscopy

Cells were fixed in 2.5% gluteraldehyde in 0.1M PBS, post-fixed in 1% osmium tetraoxide for 1hr, dehydrated in a series of increasing ethanol concentration and embedded in epoxi resin-Agar mix (Agar scientific LTD) at 60°C. Ultrathin sections were stained in uranyl acetate and lead citrate and examined in a Jeol-1200 EX transmission electron microscope (Jeol, Peabody).

Quantitative morphometrical analyses of EM images .

Quantitative evaluation of the electron micrographs was independently conducted by two observers using a scoring method previously described.[14] Means of individual observations were calculated. For morphometric evaluations, micrographs were scanned electronically. The numbers of mitochondria and granules and the area of the chromatin were recorded. Mean results were compared between patients' and healthy control neutrophils. All analyses were made in SPSS 19 using the Mann-Whitney-U test.

Immuno-blotting

Adherent cells were grown to confluence in 75cm^2 flasks. Fresh leukocytes were isolated from whole blood. Proteins were extracted by re-suspension in cold RIPA buffer containing anti-proteases. Extracts were homogenized and clarified by high-speed centrifugation. The protein concentration was determined by the Dc Protein assay (BioRad) and 20-80µg of protein were loaded onto 4–12 % Tris-Glycine gels or 12 % Bis-Tris gels. After transfer to nitrocellulose membranes (Invitrogen) blocked with 5% nonfat milk in phosphate-buffered saline or LI-COR blocking buffer (Li-Cor Biosciences), protein samples were immunoblotted with the appropriate primary antibodies, i.e., VPS45 (Abcam, Sigma-Atlas), Rabensoyn-5 and STX16 (Sigma-Atlas), Emerin (Santa Cruz Biotechnology), β-Actin (Clone AC-15; Sigma) and α-Tubulin (Sigma). For imaging, appropriate IRDye 680RD or IRDye 800CW-conjugated secondary antibodies (Li-Cor Biosciences) or peroxidase conjugated rabbit anti-goat antibodies (Jackson ImmunoResearch) were used as described. [15] Densitometry was performed on scanned immunoblot images using either, the ImageJ software as described [16] or EZquant software (EZquant, Israel).

Immuno-fluorescence

Fibroblasts were grown on cover slips and processed as described above. Peripheral blood cells were harvested and cytospan onto slides. Cells were fixed with 4% PFA and perforated with 0.05% Triton X100, washed with PBS and blocked using 5% BSA in PBS. Primary antibodies that were used were rabbit polyclonal anti-VPS45

(ProteinTech); mouse monoclonal anti-integrin beta 1 (abcam), goat poyclonal anti-Rabenosyn-5 (Santa Cruz Biotechnology), and Anti-BiP/GRP78 (BD Transduction Laboratories). Secondary antibodies included donkey anti rabbit 568 and goat anti mouse 488 (Alexa Flour). The slides were mounted using immunofluore containing DAPI (Vector Laboratories) for nuclear staining, and analyzed by fluorescent microscopy (Olympus) or laser scanning confocal microscope (Zeiss). Images were taken using the Volocity software (PerkinElmer).

Apoptosis assays

Fibroblasts were grown overnight on coverslips in 24 well plates. CaspACE FITC-VAD-FMK In Situ Marker (Promega) labeling was carried out according to the manufacturer's instructions in a final concentration of 10 μM for fluorescence microscopy viewing. Cells were fixed with 4% PFA and stained with DAPI. The percentage of apoptotic cells was calculated from the number of cells stained with activated caspase divided by cell nuclei stained with DAPI.

Caspase 3 (Active) and VPS45 immunostaining

Formalin fixed tissues were dehydrated, embedded in paraffin and sectioned at 4 μm. A positive control was added on the right side of the slides. The slides were warmed up to 60ºC for 1hr, followed by processing through a fully automated protocol. The immunostainings were calibrated on a Benchmark XT staining module (Ventana Medical Systems). Briefly, after sections were dewaxed and rehydrated, a CC1 Standard Benchmark XT pretreatment for antigen retrieval (Ventana Medical Systems) was

selected for both antibodies Caspase 3 (Active) and VPS45 (ProteinTech). Caspase 3 (Active) antibody (Epitomics, California, 1476-1) was diluted 1:10 and VPS45 (ProteinTech, Chicago, 12006-1-AP) was at 1: 20. Caspase 3 (Active) was incubated 1 hr at 37ºC and VPS45 30 min. Detection was performed with ultraView detection kit (Ventana Medical Systems) and counterstained with hematoxylin (Ventana Medical Systems). After the run on the automated stainer was completed, the slides were dehydrated in a serie of increasing ethanol concentration. The sections were cleared in xylene for 10 seconds and mount with Entellan (Merck). The stained sections were viewed and imaged with a light microscope and analyzed by a pathologist.

Real-time quantitative PCR assays

To isolate total RNA, 2-4 X 10^6 cells were harvested using Trizol according to the manufacturer's instructions. cDNA was made from 1 μg of total RNA using the cDNA Archive kit (Applied Biosystems). Real-time PCR was performed using an ABI 7900 Sequence Detection System (Applied Biosystems). Primers and probes for HSPA5/BiP mRNA, a marker of endoplasmic reticulum stress, were obtained as assays on demand from Applied Biosystems. For each analysis, transcription of the gene of interest was compared with transcription of the TBP or GAPDH reference gene that was amplified in parallel. The samples were analyzed in triplicate, and fold changes in transcription were calculated by using the ΔΔCt comparative method. In all experiments, equal amounts of fibroblast cDNA were used.

Zebrafish studies

Wild type zebrafish (*Danio rerio*) of genetic strain Ekkwill (EK) were housed and maintained in an Association for assessment and accreditation of laboratory animal care (AAALAC) accredited animal facility at NHGRI under an Animal Care and Use Committee (ACUC) approved animal protocol (#G05-5). Pigmentation in embryos older than 24 hpf was inhibited either using PTU (I-phenyl-2-thiourea; Sigma) as described[17] or by bleaching in a 0.5 × SSC, 5% formamide, 10% H_2O_2 solution. [18] The high-resolution in situ hybridization to whole-mount zebrafish embryos was performed with BM purple AP substrate (Roche) instead of NBP and BCIP.

Morpholino sequences: ATG morpholino: CAGCAAGAGTCACGTTCATTTTGGC

Splicing morpholino (I2E3): TCTCCTGAAATCAAAGAGGGTGTGA

SUPPLEMENTARY FIGURES AND LEGENDS

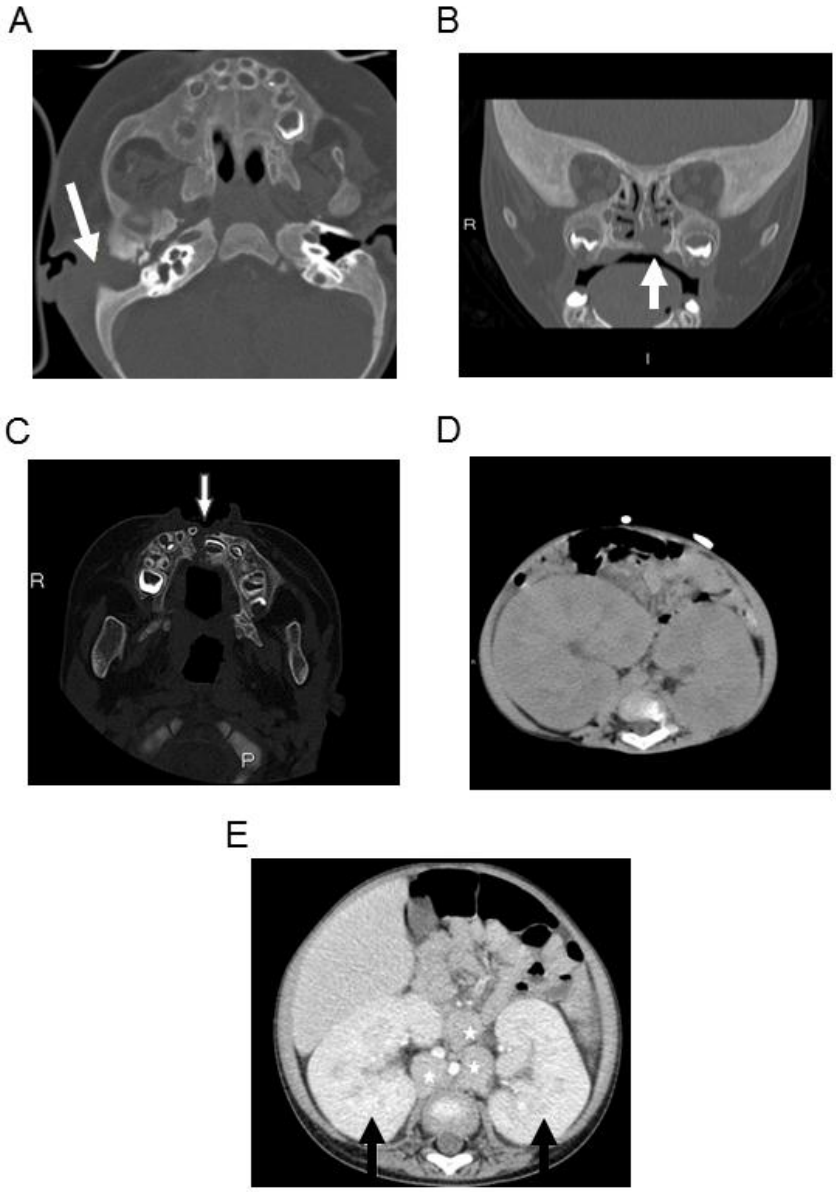

Fig. S1. Imaging studies.

A. CT scan of paranasal sinuses and facial bones image of patient B-II-10 showing destructive lesion of right mastoid bone (arrow) and adjacent soft tissue swelling. **B-C.** Coronal (B) and axial (C) CT images of patient C-II-3 demonstrating destructive lesion of hard palate (arrow) and destructive lesion of alveolar ridge (arrow), respectively. **D.** Axial abdominal CT image of patient A-II-3 showing gross enlargement of both kidneys. **E.** Contrast enhanced abdominal CT scan of patient B-II-9 demonstrating retroperitoneal lymphadenopathy (asterisks) and bilateral enlarged kidneys (arrows).

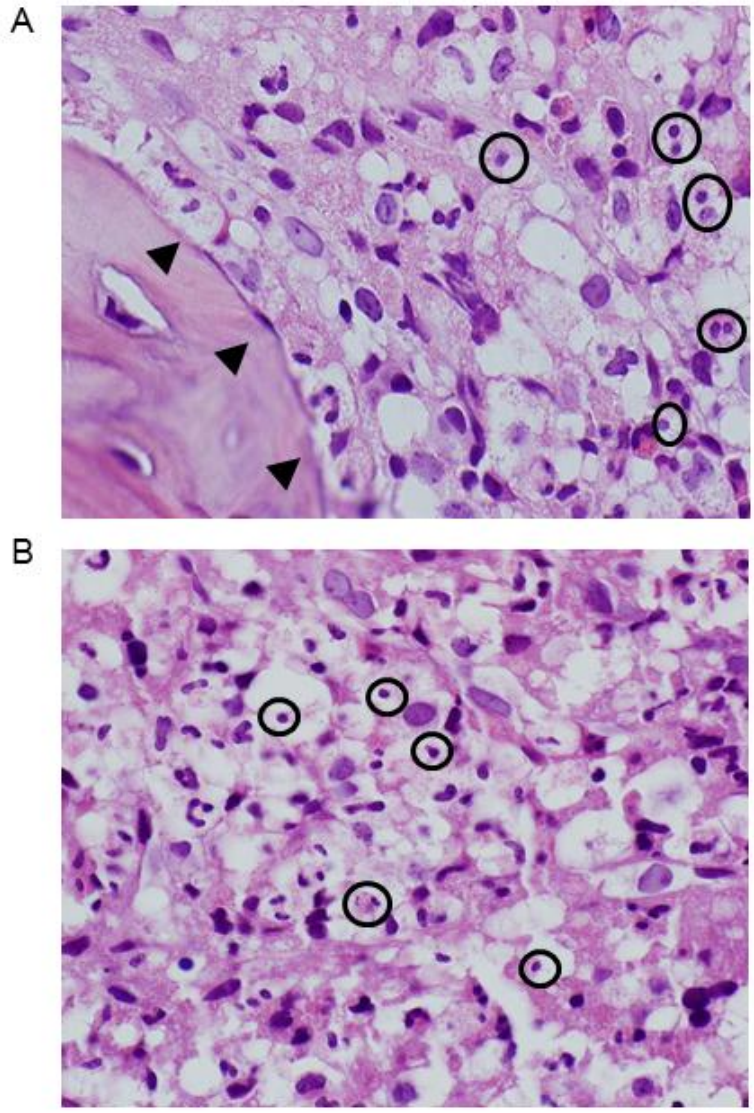

Fig. S2. Bone marrow biopsy.

Neutrophils and bands are localized near the bone (arrowheads). Some neutrophils show defective nuclear segmentation with one or two separate nuclear lobules and no obvious connecting interlobular chromatin filaments (circles). Part of the monolobated cells represents apoptotic cells. (**A**, H&E x1000,). Inter-trabecular area of bone marrow demonstrates numerous apoptotic pycnotic nuclei (circles) (**B**, H&E x1000).

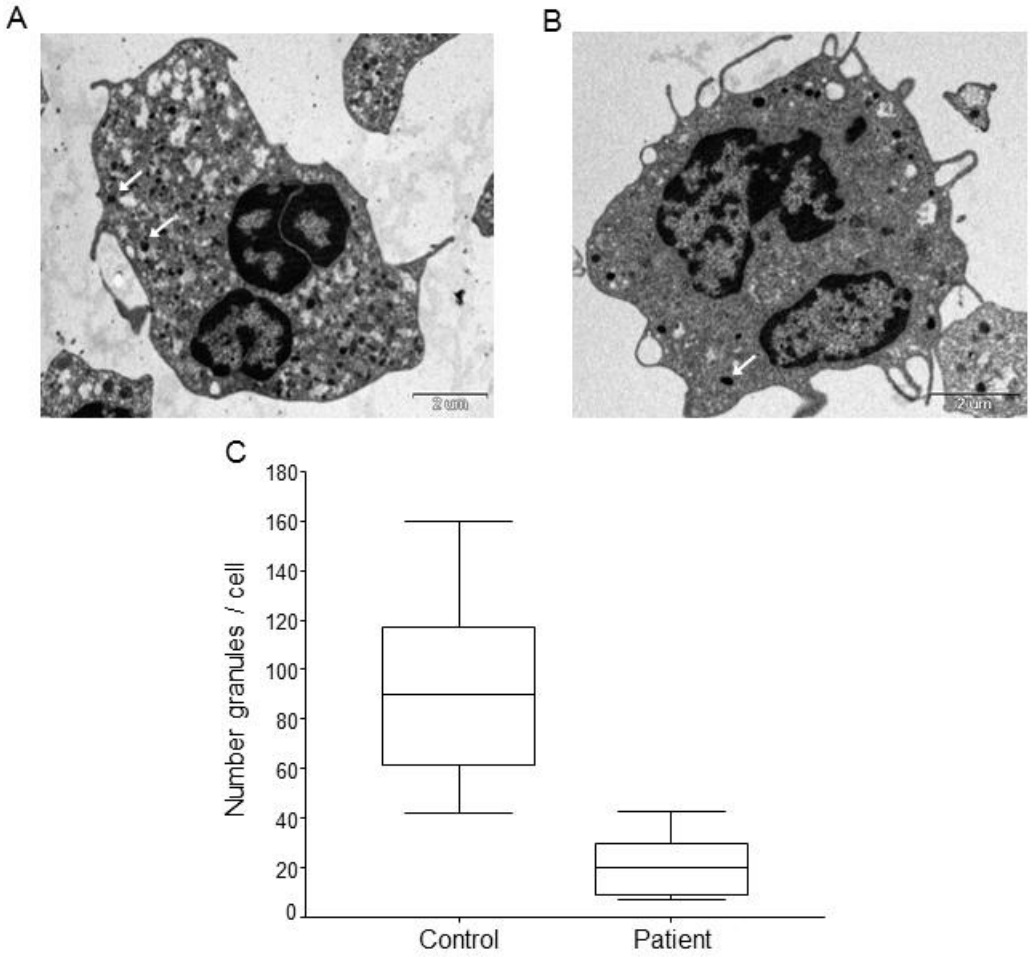

Fig. S3, I-III. Electron micrographs and morphometric analyses of electron microscopic (EM) images of patients' and healthy control neutrophils.

Fig. S3-I. Granule numbers.

Representative EM images of patient and healthy control neutrophils indicating low (**B**) and high (**A**) granule numbers, respectively. Granules were counted and SPSS statistical analysis was performed (**C**). Control: median = 90 (IQR = 60.75-120.25); n = 8. Patient: median = 20 (IQR = 8-30); n = 11. $P<0.001$. The graphs indicate the interquartile range of the measurements. The dashed line represents the median value.

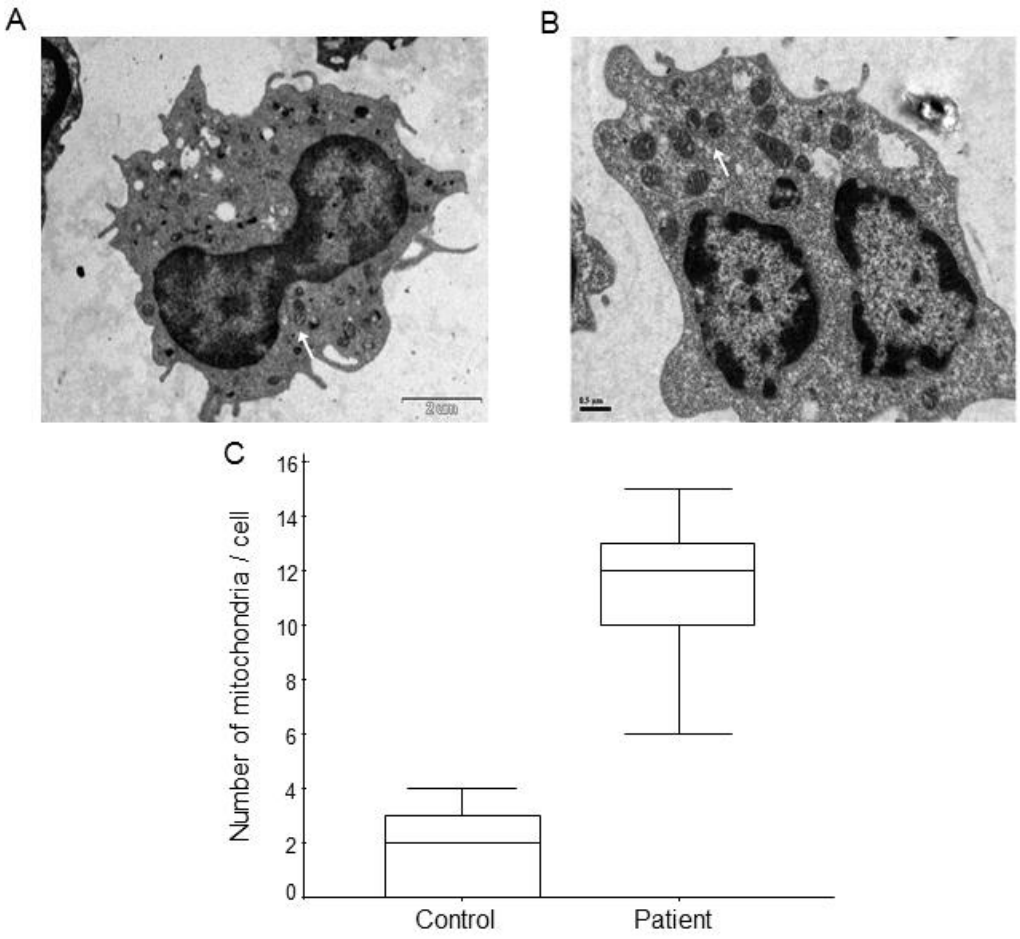

Fig. S3-II. Mitochondria.

Representative EM images of neutrophils showing abundant mitochondria in patient's cell (**B**) compared with healthy control (**A**). Mitochondria were counted and SPSS statistical analysis was performed (**C**). Control: median = 2 (IQR = 0-3); n = 13. Patient: median = 12 (IQR = 9.5-13); n = 13. $P<0.001$. The graphs indicate the interquartile range of the measurements. The dashed line represents the median value.

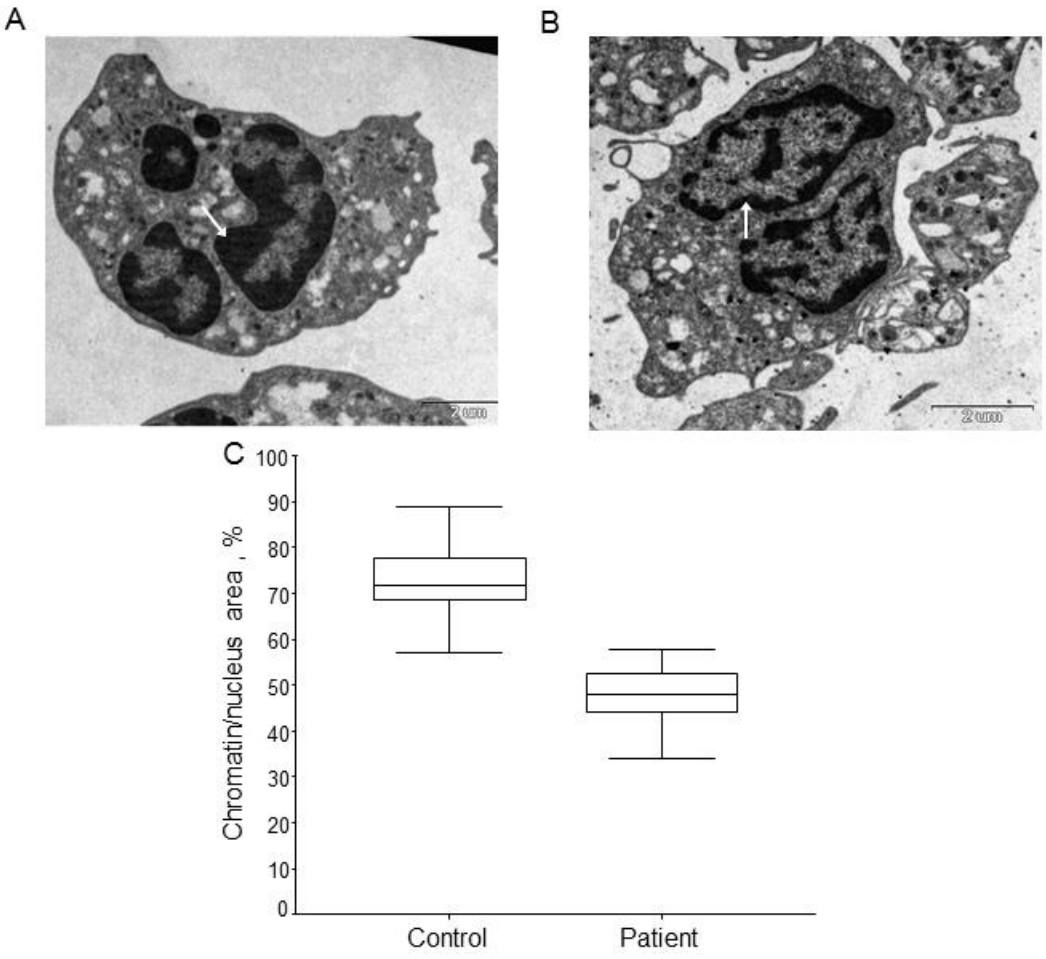

Fig. S3-III. Chromatin area.

Representative EM images of patient and healthy control neutrophils indicating uncondensed (**B**) and condensed (**A**) chromatin, respectively. Chromatin area was calculated using Image J program and SPSS statistical analysis was performed (**C**). Results are presented in arbitrary units. Control: median = 71.7 (IQR = 67-78); n = 19. Patient: median = 48.1 (IQR = 44-53); n = 22. P<0.001. The graphs indicate the interquartile range of the measurements. The dashed line represents the median value.

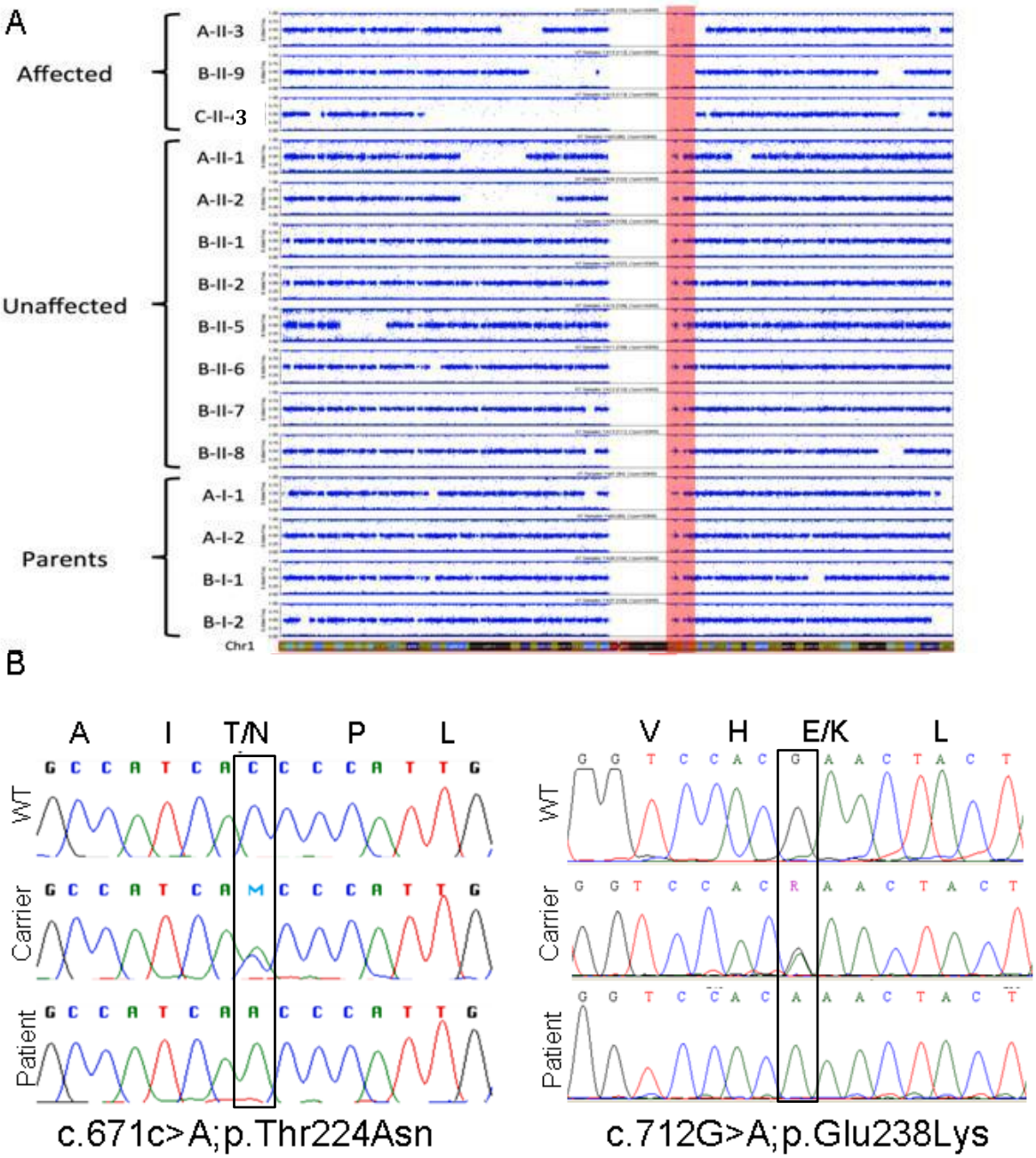

Fig. S4. Genetic data.

A. SNP-array data (B-allele frequency plots) of chromosome 1 for 3 patients and their family members. The middle of the B allele plots represents heterozygosity (AB) and the upper and lower edges represent homozygosity (AA or BB). Highlighted in red is the region of homozygosity shared by affected individuals. **B.** Mutation validation. Chromatograms of the different genotypes observed for the c.671C>A; p.Thr224Asn and the c.712G>A; p. Glu238Lys mutations.

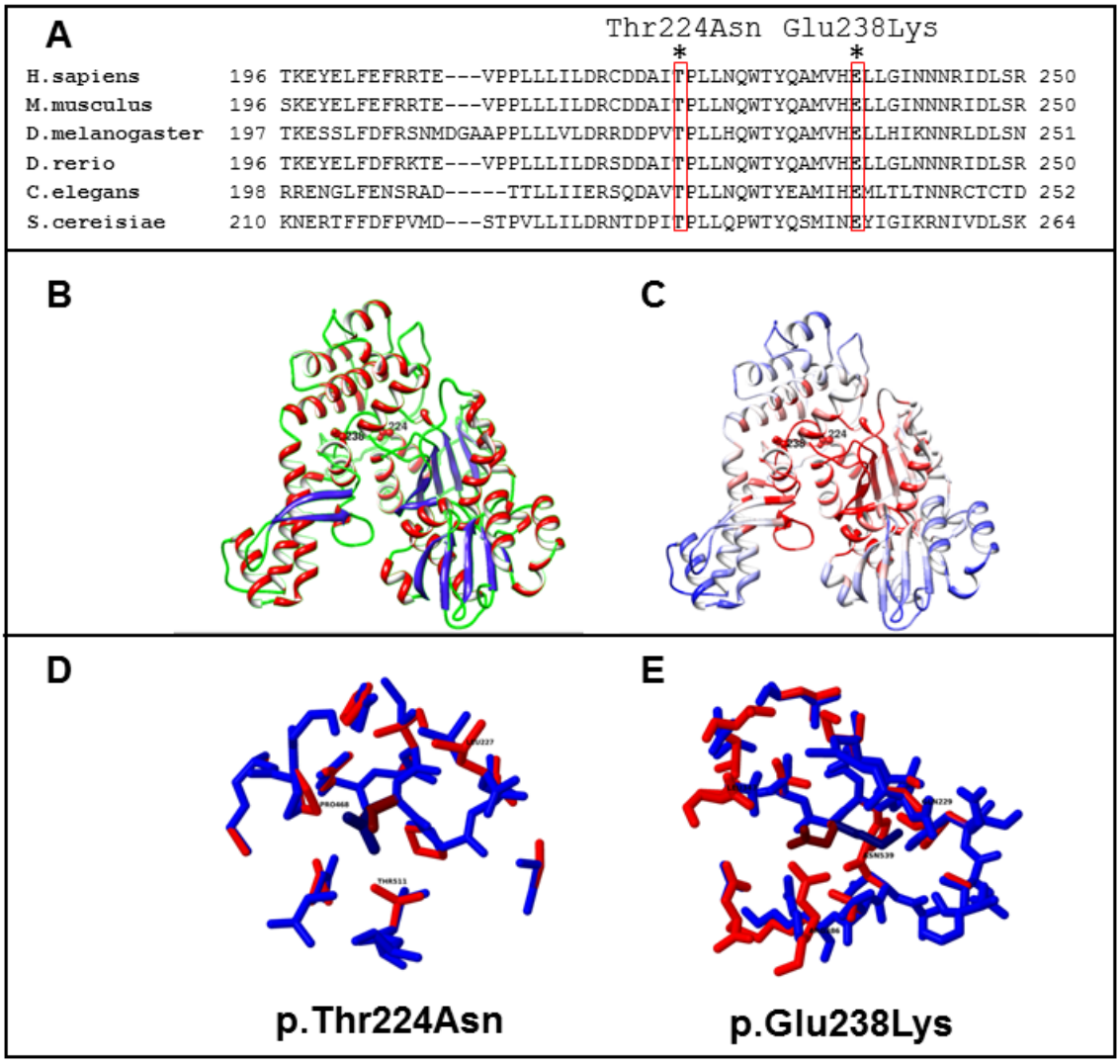

Fig. S5. Structural models of VPS45 and mutated residues.

A. Evolutionary conservation of the mutated Thr224 and Glu238 residues. **B**. Cartoon view of the overall structure of the protein, colored by secondary structure elements. Thr224 and Glu238 residues appear in ball and stick representation and labeled. **C**. Coloring according to the closeness index of SARIG. [19] Reddish colors indicate centrality in the spatial network of residues. Thr224 and, to a lesser extent, Glu238 have high closeness index. **D**. Modeling of the Thr224Asn mutant. Several residues, such as P468, T511 and L227 undergo conformational change. Thr224 appears in darker colors in the center. Red: wild type structure, Blue: Thr224Asn mutant. **E.** Modeling of the Glu238Lys mutant.

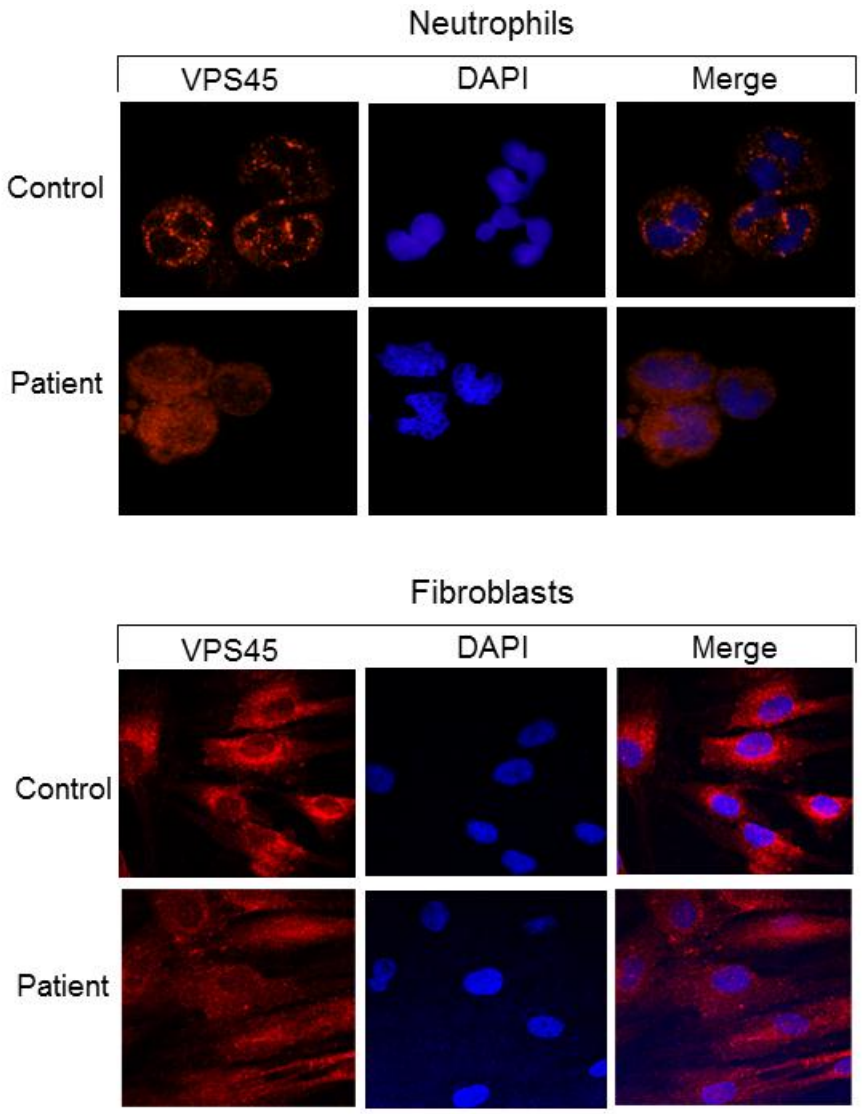

Fig. S6. Immuno-fluorescence studies of VPS45

Immuno-fluorescence studies show a punctate, cytoplasmic, predominantly perinuclear distribution of VPS45 (red) in normal neutrophil (upper panel) and fibroblasts (lower panel). VPS45 in neutrophils and fibroblasts of patient B-II-10 appears reduced and has a more diffuse cellular distribution. Nuclei (Dapi) stain blue.

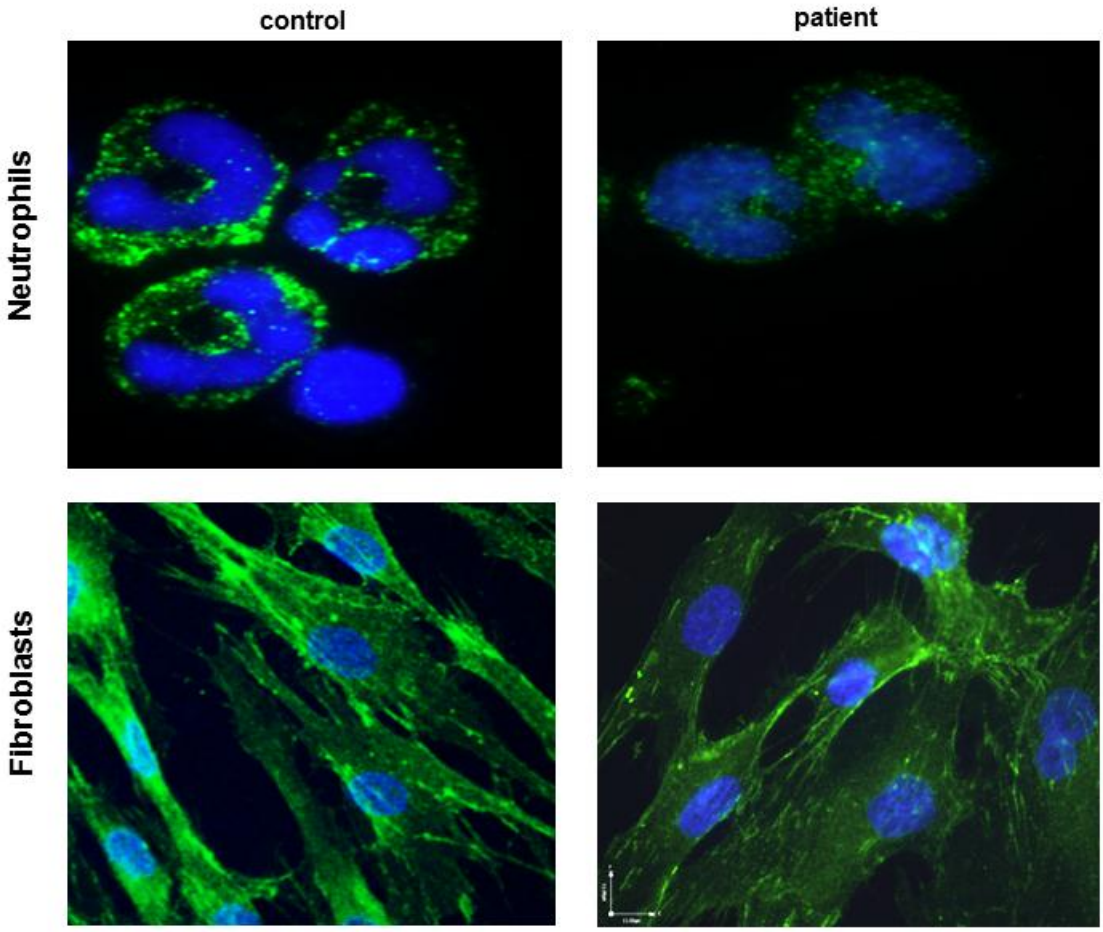

Fig. S7. Immuno-fluorescence studies of β1 integrin.

Immuno-fluorescence of β1 integrin in neutrophils (upper panel) and fibroblasts (lower panel) is shown. Patient has less staining compared to control. β1 integrin stains green and the nuclei (DAPI) stain blue**.**

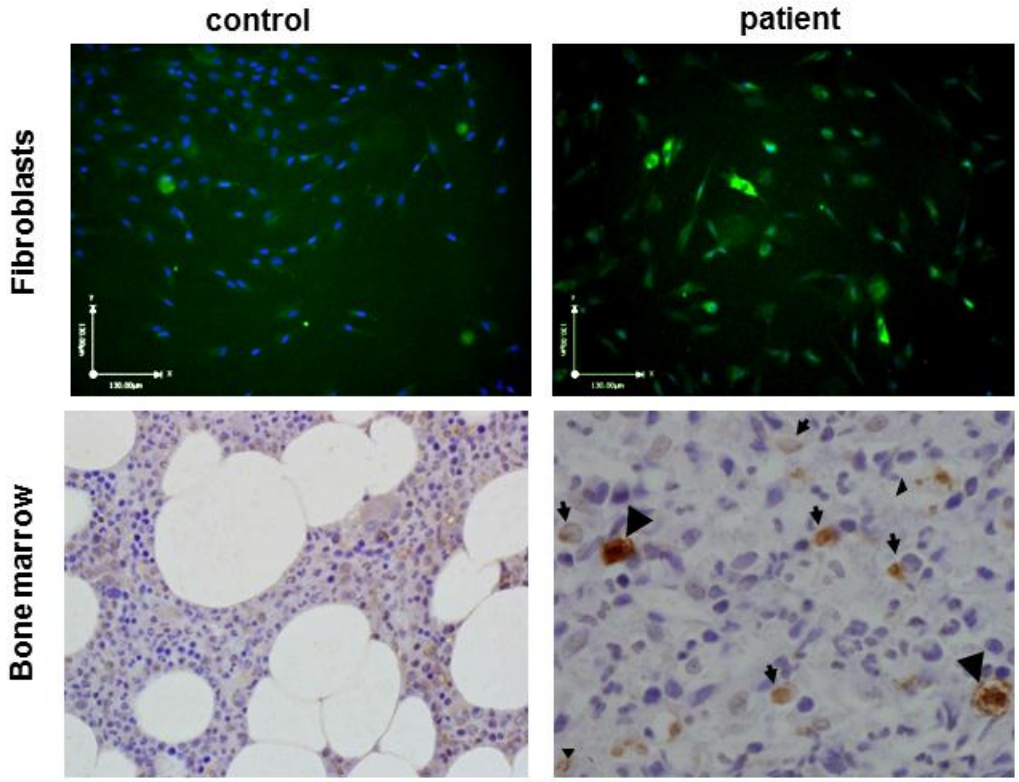

Fig. S8. Apoptosis in patient and control fibroblasts and bone marrow.
Fibroblast staining with activated caspase-3 (green) marker for apoptosis, display an increase in cell-positivity in patient compared to control (upper panel). Bone marrow cells of VPS45-deficient patient show abundant staining for Caspase 3 (arrows) indicative of enhanced apoptosis (lower panel, H&E x600). The two strongly positive large-looking cells are neutrophils with nuclear and cytoplasmic staining. The less strongly stained cells are immature white cells and the smaller ones are apoptotic bodies. In normal bone marrow obtained from control (left), composed of hematopoietic stem cells and fat, staining with caspase 3 revealed no positive apoptotic cells (H&E x400).

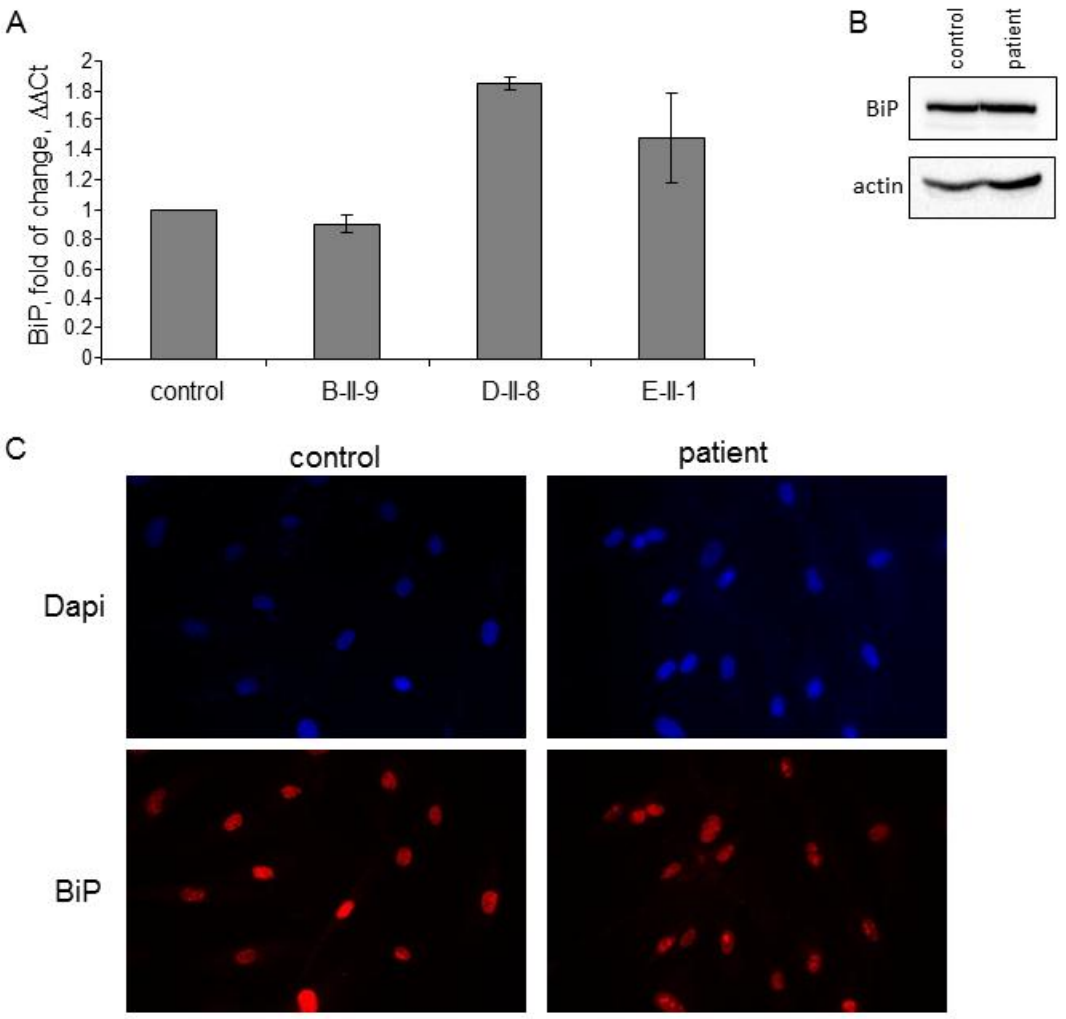

Fig. S9. BiP expression

Endoplasmic reticulum stress, determined by the RNA expression (**A**) and the protein level (**B,C**) of BiP in patients' and controls' fibroblast cells, was assessed. For RQ-PCR, the expression of BiP was measured in parallel with the expression of TBP (TATA-binding protein) reference gene. In all methods used; RQ-PCR (**A**), western blot analysis (**B**) and immuno-fluorescence (**C**) no significant changes were observed between patient and control samples.

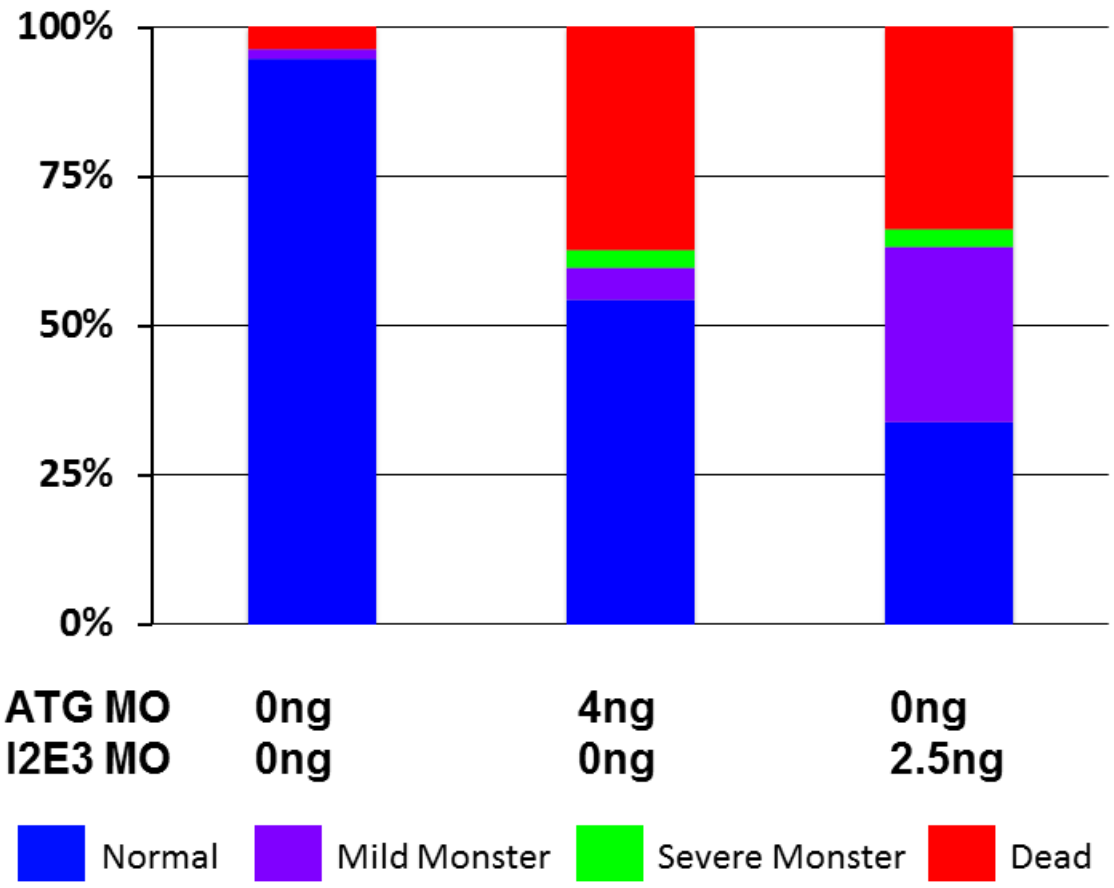

Fig. S10. Toxicity of the morpholinos.

Effect of the two morpholinos on zebrafish embryos at 5 days post-fertilization (dpf). Percentage of control and injected zebrafish in the 4 different toxicity phenotypes [20] (Normal, Mild Monster, Severe Monster and Dead) is shown.

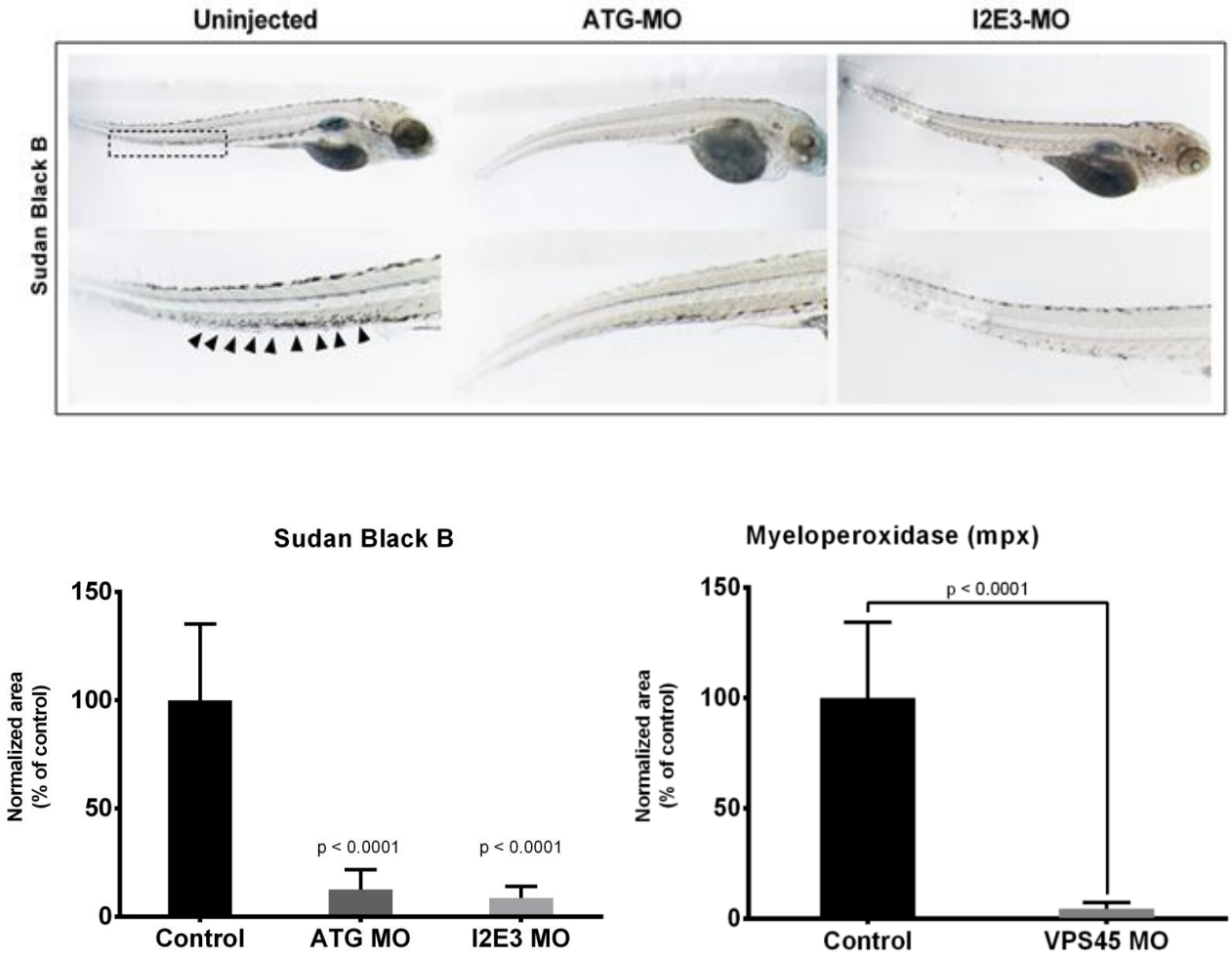

Fig. S11. Sudan Black B and myeloperoxidase analyses of zebrafish embryos

Sudan Black B staining on 5dpf embryos supports functional knockdown of vps45. Representative images are shown: uninjected zebrafish embryos (left); embryos injected with ATG-MO (middle); and embryos injected with I2E3-MO (right).

Sudan Black B staining positive cells are marked by rectangle or arrowheads in the uninjected embryos. Injection of either ATG-MO or I2E3-MO revealed a marked reduction in the number of Sudan-Black-positive neutrophils. Densitometric analysis (lower panel) of the Sudan Black B (left) and myeloperoxidase (right) staining levels in morpholino-injected embryos are shown below the images. Data are expressed as mean percentage ±SD relative to uninjected embryos (control). All experiments were done in triplicate. N = 30 embryos. The *P* values are computed between uninjected control and morpholino-injected embryos.

Table S1. Protein-changing variants identified in patient B-II-9, genes located in the candidate region

Chromosome	Gene name	Mutation type	Nucleotide				Amino-acid		
			Left flank	Right flank	Reference	Variant	Position	Reference	Variant
chr1	*VPS45*	Nonsynonymous	148316464	148316466	C	A	224	T	N
chr1	*HRNR*	Nonsynonymous	150452767	150452769	C	T	2654	S	N
chr1	*HRNR*	Nonsynonymous	150453113	150453115	C	T	2539	G	S
chr1	*HRNR*	Nonsynonymous	150453148	150453150	C	T	2527	R	Q
chr1	*HRNR*	Nonsynonymous	150455860	150455862	C	G	1623	S	T
chr1	*HRNR*	Nonsynonymous	150455933	150455935	C	T	1599	G	S
chr1	*HRNR*	Nonsynonymous	150455968	150455970	C	T	1587	R	Q
chr1	*HRNR*	Nonsynonymous	150455978	150455980	C	T	1584	G	S
chr1	*HRNR*	Nonsynonymous	150456953	150456955	C	T	1259	G	S
chr1	*HRNR*	Nonsynonymous	150457270	150457272	C	G	1153	S	T
chr1	*HRNR*	Nonsynonymous	150457378	150457380	C	T	1117	R	Q
chr1	*HRNR*	Nonsynonymous	150457388	150457390	C	T	1114	G	S
chr1	*HRNR*	Nonsynonymous	150457552	150457554	T	A	1059	Q	L
chr1	*NUP210L*	Nonsynonymous	152328605	152328607	T	G	759	H	P

Table S2. Prediction of changes in stability and function of VPS45 Thr224Asn and Glu238Lys mutation using various computational tools.

Program	Sequence/Structure Approach	Thr224Asn Stability change (ΔΔG) and comments*	Glu238Lys Stability change (ΔΔG) and comments*	URL
eris[21]	structure	destabilize (+2.18)	destabilize (+2.14)	http://dokhlab.unc.edu/tools/eris
cupsat[22]	structure	destabilize (+5.21)	destabilize (+1.86)	http://cupsat.tu-bs.de
Popmusic[23]	structure	destabilize (+1.08)	destabilize (+0.90)	http://babylone.ulb.ac.be/popmusic/
Foldx[24]	structure	destabilize (+1.53)	destabilize (+0.84)	http://foldx.crg.es/
MUpro[25]	structure (NN)	destabilize confidence score 0.534	destabilize confidence score -0.302	http://www.ics.uci.edu/~baldig/mutation.html
	structure (SVM)	destabilize	destabilize	
	sequence (SVM)	stabilize confidence score 0.128	stabilize confidence score 0.295	
MuStab[26]	sequence	destabilize confidence score 0.854	destabilize confidence score 0.805	http://bioinfo.ggc.org/mustab/

SDM[27]	structure	destabilize (+0.85) "non-disease associated"	destabilize (+2.63) highly destabilizing and cause protein malfunction	http://mordred.bioc.cam.ac.uk/sdm/sdm.php
auto-mute[28]	structure (REPTree)	destabilize (+1.34)	destabilize (+0.81)	http://proteins.gmu.edu/automute/AUTO-MUTE_Stability_ddG_Details.html
	structure (SVM reression)	destabilize (+1.15)	destabilize (+1.15)	
	structure (random forest)	destabilize confidence score 0.69	destabilize confidence score 0.77	
	structure (SVM)	destabilize confidence score 0.88	destabilize confidence score 0.88	
Mutpred[29]	sequence	destabilize probability for deleterious mutation 0.935	destabilize probability for deleterious mutation 0.918	http://mutpred.mutdb.org
PolyPhen2[30]	sequence	destabilize probably damaging mutations	destabilize probably damaging mutations	http://genetics.bwh.harvard.edu/pph2/index.shtml
ProSMS	sequence 3 state prediction	destabilize	destabilize	http://babel.ucmp.umu.se/prosms/index.php
SNAP[31]	sequence	non-neutral functional change	non-neutral functional change	http://rostlab.org/services/snap/

*stability change - kcal/mol. Positive value means that the mutation thermodynamically destabilizes the protein.
NN: Neuronal Network, SVM: Support Vector Machine

References

1. Bentley DR, Balasubramanian S, Swerdlow HP, et al. Accurate whole human genome sequencing using reversible terminator chemistry. Nature 2008;456:53-9.
2. Teer JK, Mullikin JC. Exome sequencing: the sweet spot before whole genomes. Hum Mol Genet 2010;19:R145-51.
3. Teer JK, Green ED, Mullikin JC, Biesecker LG. VarSifter: visualizing and analyzing exome-scale sequence variation data on a desktop computer. Bioinformatics 2012;28:599-600.
4. Gnirke A, Melnikov A, Maguire J, et al. Solution hybrid selection with ultra-long oligonucleotides for massively parallel targeted sequencing. Nat Biotechnol 2009;27:182-9.
5. Livak KJ, Schmittgen TD. Analysis of relative gene expression data using real-time quantitative PCR and the 2(-Delta Delta C(T)) Method. Methods 2001;25:402-8.
6. Burkhardt P, Stegmann CM, Cooper B, et al. Primordial neurosecretory apparatus identified in the choanoflagellate Monosiga brevicollis. Proc Natl Acad Sci USA 2011;108:15264-9.
7. Eswar N, Webb B, Marti-Renom MA, et al. Comparative protein structure modeling using Modeller. Current protocols in bioinformatics / editoral board, Andreas D Baxevanis [et al] 2006;Chapter 5:Unit 5 6.
8. Sali A, Blundell TL. Comparative protein modelling by satisfaction of spatial restraints. J Mol Biol 1993;234:779-815.
9. Eyal E, Najmanovich R, McConkey BJ, Edelman M, Sobolev V. Importance of solvent accessibility and contact surfaces in modeling side-chain conformations in proteins. J Comput Chem 2004;25:712-24.
10. Jmol: an open source Java viewer for chemical structures in 3D. http://www.jmol.org/ (Accessed at http://www.jmol.org/)
11. Pettersen EF, Goddard TD, Huang CC, et al. UCSF Chimera--a visualization system for exploratory research and analysis. J Comput Chem 2004;25:1605-12.
12. Ben-Ari J, Wolach O, Gavrieli R, Wolach B. Infections associated with chronic granulomatous disease: linking genetics to phenotypic expression. Expert Rev. Anti Infect. Ther 2012;10:881-94.
13. Wolach B, Gavrieli R, Roos D, Berger-Achituv S. Lessons learned from phagocytic function studies in a large cohort of patients with recurrent infections. J Clin Immunol 2012;32:454-66.
14. Bishop JB, Tani Y, Witt K, et al. Mitochondrial damage revealed by morphometric and semiquantitative analysis of mouse pup cardiomyocytes following in utero and postnatal exposure to zidovudine and lamivudine. Toxicological sciences : an official journal of the Society of Toxicology 2004;81:512-7.
15. Madeira da Silva L, Vandepas L, Bianco SD. Mutagenesis and analysis of genetic mutations in the GC-rich KISS1 receptor sequence identified in humans with reproductive disorders. J Vis Exp 2011:e2897.
16. Chapman MD, Keir G, Petzold A, Thompson EJ. Measurement of high affinity antibodies on antigen-immunoblots. J Immunol Methods 2006;310:62-6.

17. Westerfiled M. The Zebrafish book. A guide for the laboratory use of zebrafish (Danio rerio): University of Oregon; 2000.
18. Thisse C, Thisse B. High-resolution in situ hybridization to whole-mount zebrafish embryos. Nat Protoc 2008;3:59-69.
19. Amitai G, Shemesh A, Sitbon E, et al. Network analysis of protein structures identifies functional residues. J Mol Biol 2004;344:1135-46.
20. Bedell VM, Westcot SE, Ekker SC. Lessons from morpholino-based screening in zebrafish. Brief Funct Genomics 2011;10:181-8.
21. Yin S, Ding F, Dokholyan NV. Eris: an automated estimator of protein stability. Nat Methods 2007;4:466-7.
22. Parthiban V, Gromiha MM, Schomburg D. CUPSAT: prediction of protein stability upon point mutations. Nucleic Acids Res 2006;34:W239-42.
23. Dehouck Y, Kwasigroch JM, Gilis D, Rooman M. PoPMuSiC 2.1: a web server for the estimation of protein stability changes upon mutation and sequence optimality. BMC Bioinformatics 2011;12:151.
24. Guerois R, Nielsen JE, Serrano L. Predicting changes in the stability of proteins and protein complexes: a study of more than 1000 mutations. J Mol Biol 2002;320:369-87.
25. Cheng J, Randall A, Baldi P. Prediction of protein stability changes for single-site mutations using support vector machines. Proteins 2006;62:1125-32.
26. Teng S, Srivastava AK, Wang L. Sequence feature-based prediction of protein stability changes upon amino acid substitutions. BMC Genomics 2010;11 Suppl 2:S5.
27. Worth CL, Preissner R, Blundell TL. SDM--a server for predicting effects of mutations on protein stability and malfunction. Nucleic Acids Res 2011;39:W215-22.
28. Masso M, Vaisman, II. AUTO-MUTE: web-based tools for predicting stability changes in proteins due to single amino acid replacements. Protein Eng Des Sel 2010;23:683-7.
29. Li B, Krishnan VG, Mort ME, et al. Automated inference of molecular mechanisms of disease from amino acid substitutions. Bioinformatics 2009;25:2744-50.
30. Adzhubei IA, Schmidt S, Peshkin L, et al. A method and server for predicting damaging missense mutations. Nat Methods 2010;7:248-9.
31. Bromberg Y, Rost B. SNAP: predict effect of non-synonymous polymorphisms on function. Nucleic Acids Res 2007;35:3823-35.